Supplement of Earth Syst. Dynam., 11, 161–181, 2020
https://doi.org/10.5194/esd-11-161-2020-supplement

Earth System Dynamics
Open Access
EGU

Supplement of

Changes in the future summer Mediterranean climate: contribution of teleconnections and local factors

Monika J. Barcikowska et al.

Correspondence to: Monika J. Barcikowska (mjbarcikowska@gmail.com)

Supplementary Material

Fig SI1. Spatial pattern of SNAO, derived from the 20CR reanalysis, derived from periods: 1851-1890, 1891-1930, 1931-1970, 1971-2010.

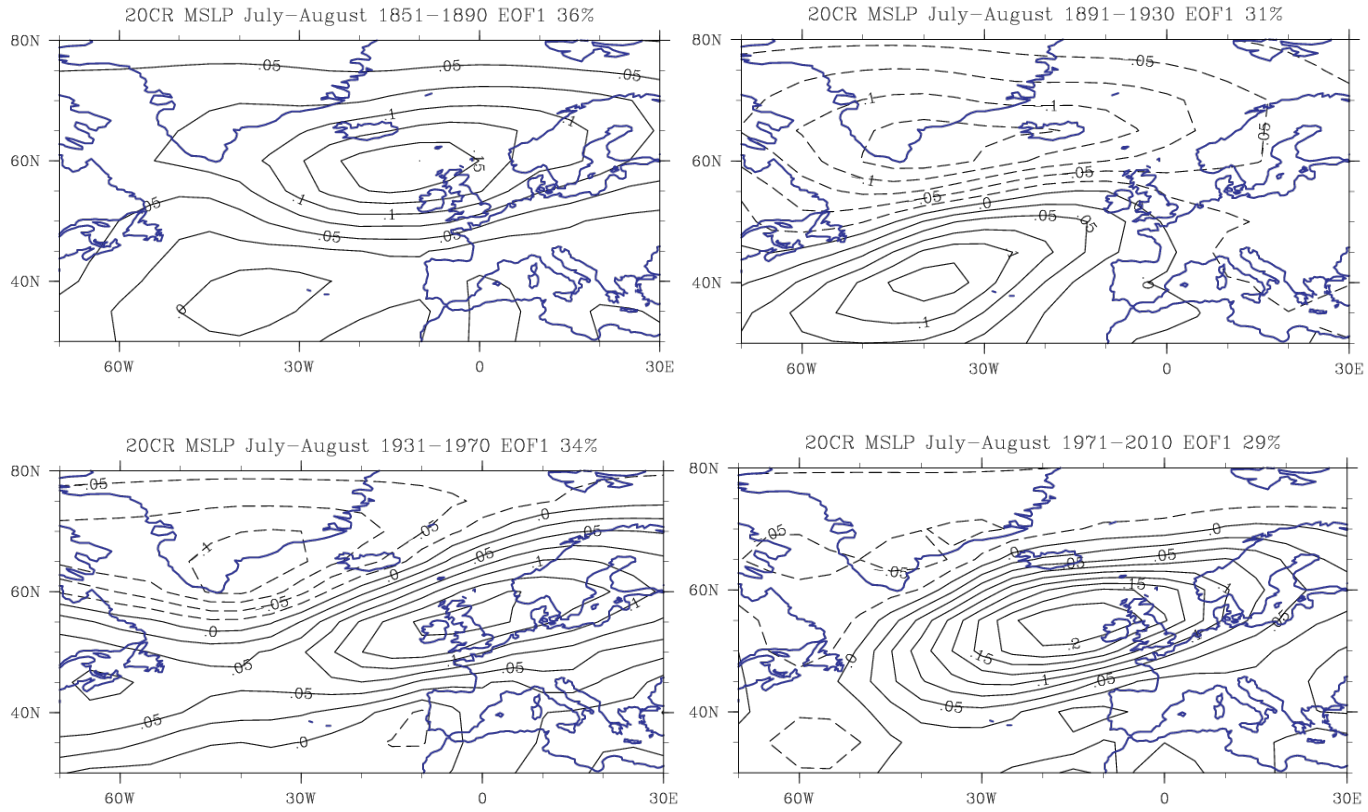

Fig S2. Spatial patterns of the SNAO using SLP, derived from five HIST runs in 1870-1920 (left column), and 1960-2010 (right column). The pattern is shown as correlations between time series of the first PC of SLP and SLP fields in July-August. The sign of each derived EOF is arbitrary, but here the signs were converted to match the SNAO at its negative phase.

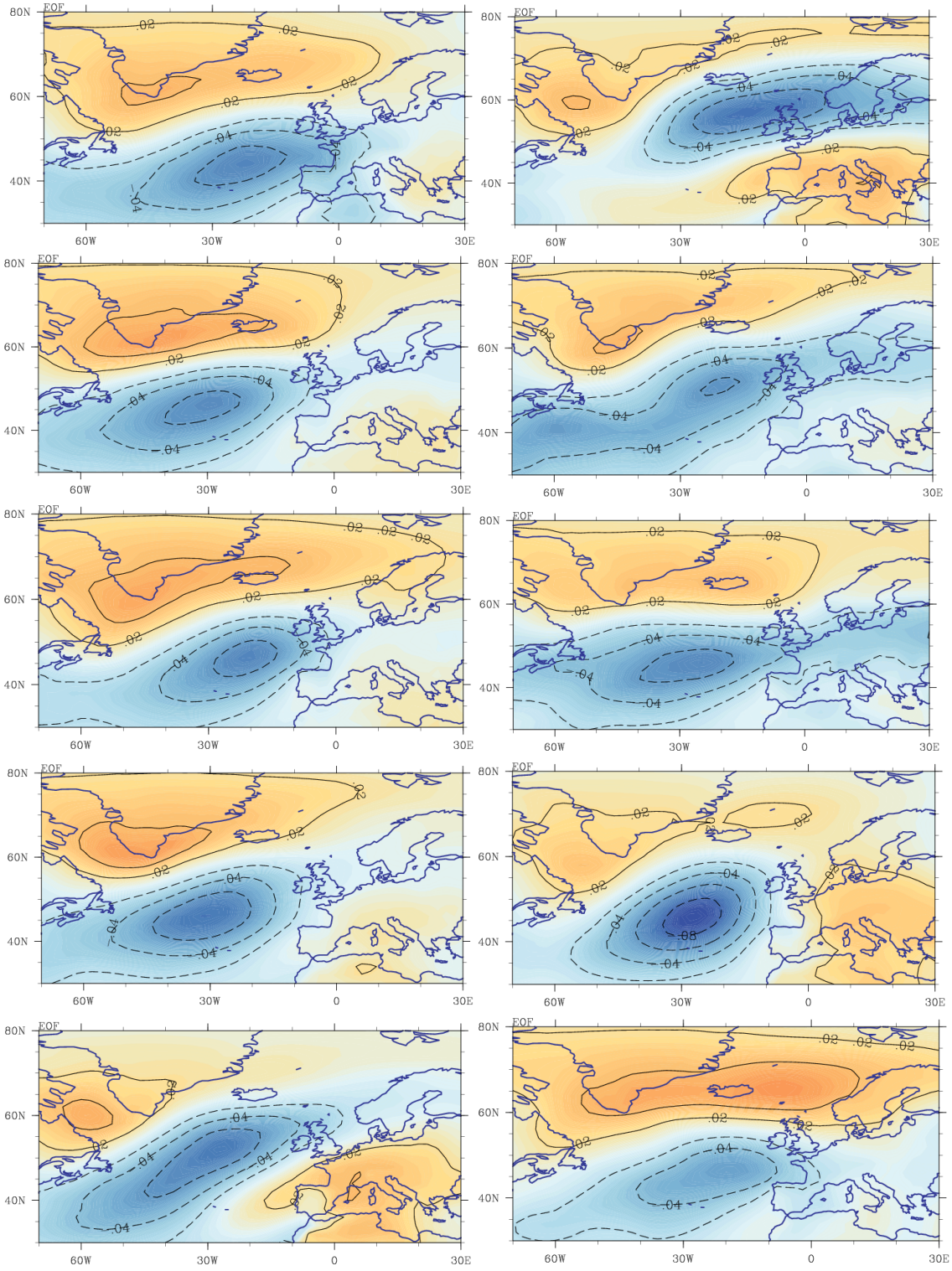

Fig S3. Spatial pattern of SNAO using SLP derived from the period 1970-2030 in the five HIST+PROJ runs. The pattern is shown as correlations between the principal component time series of the first EOF of SLP and SLP fields in July-August.

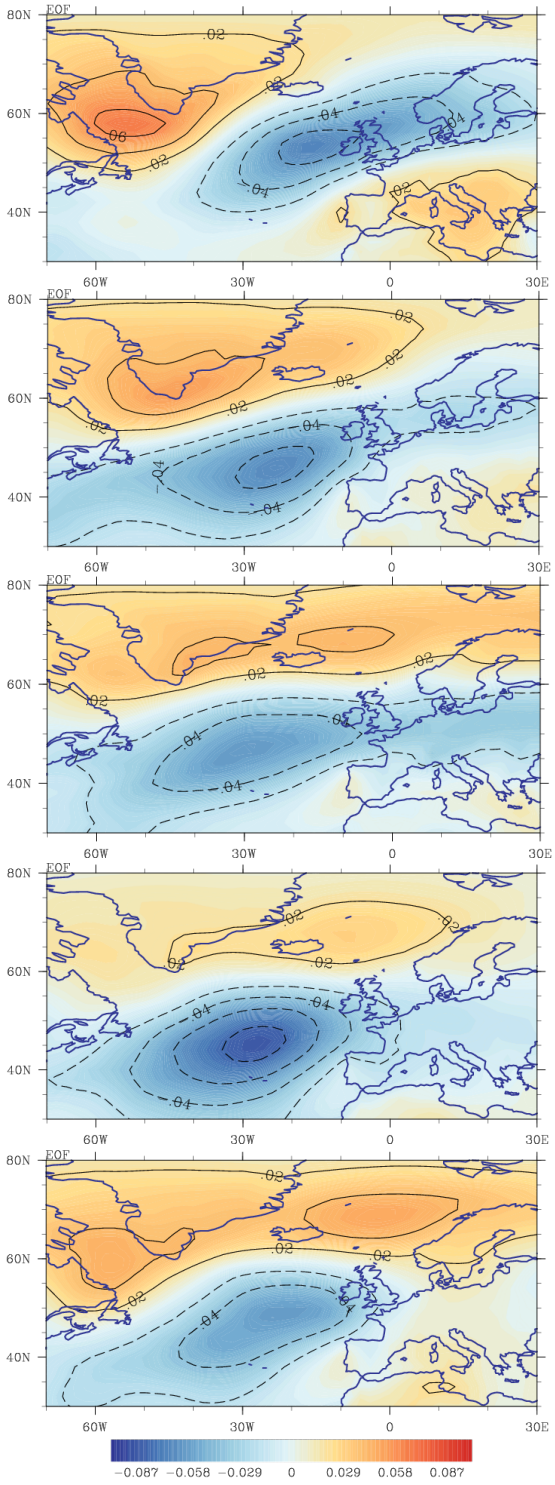

Fig S4. Future changes projected for vertical velocities at a) 500 hPa, c) 600 hPa, e) 700 hPa in JJA and in July in b), d), f) respectively. The changes are derived in the period 2061-2099 and compared with the baseline period 1961-1999, derived at the original horizontal resolution (~0.25°). The vertical axis is oriented downward, i.e. negative tendencies (in blue) indicate upward motion while positive tendencies (red, stronger subsidence) indicate downward motion.

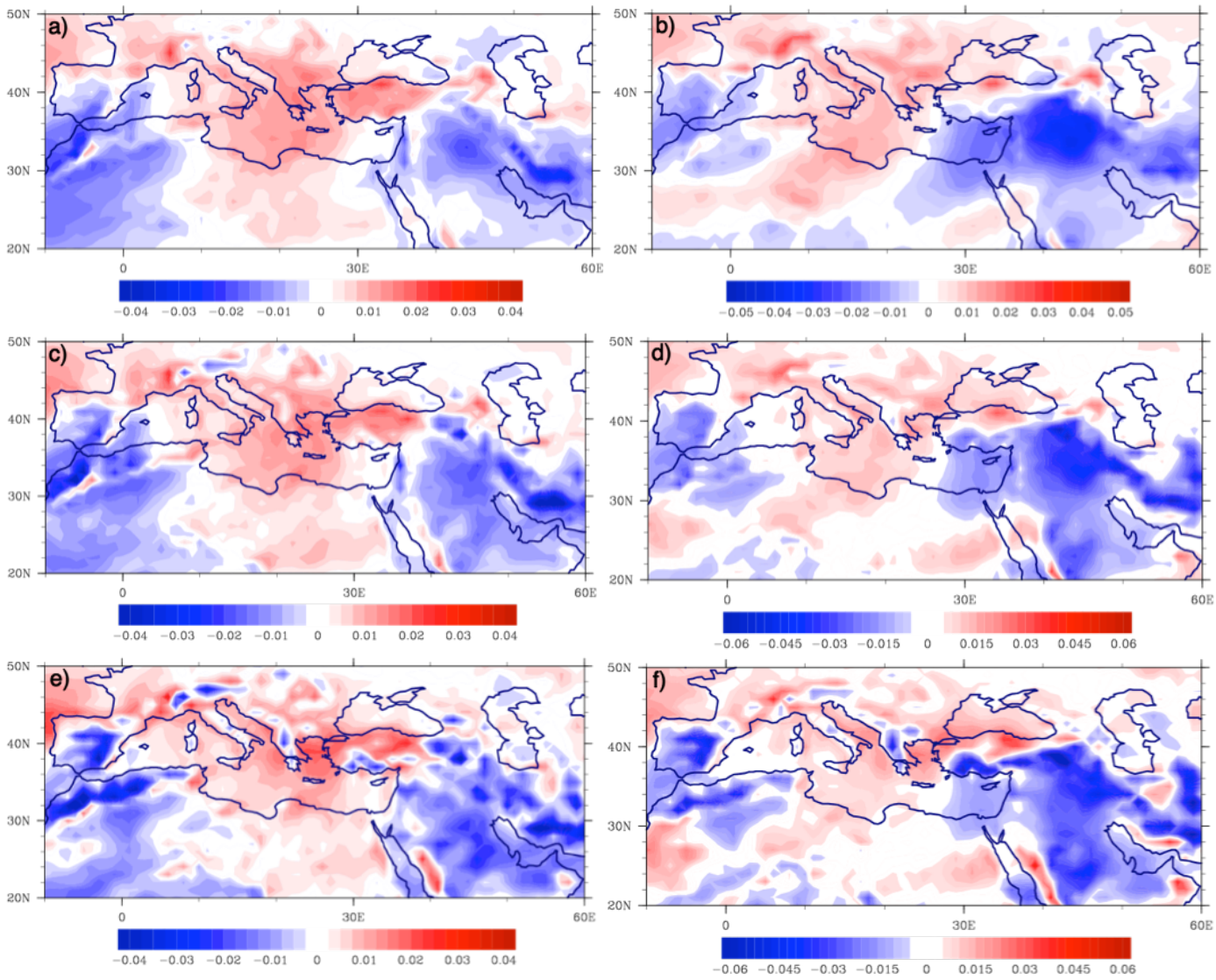

Figure S5. Projected future changes for the summer (JJA) surface temperature (left,°C), and precipitation (right, mm/day) based on the 10-member ensemble simulations of the CSIRO-Mk3-6-0 model, for the forcing scenario RCP8.5.

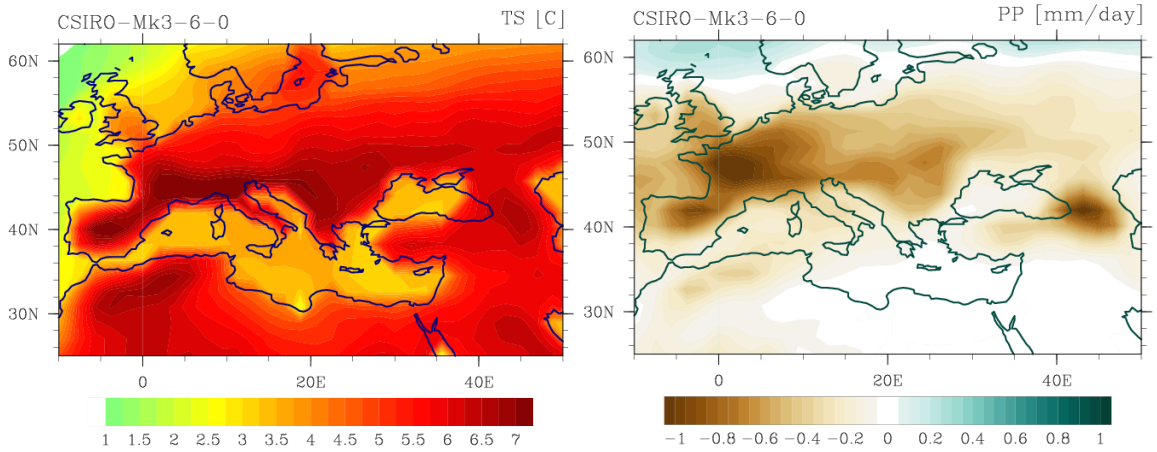

Fig S6. As in Fig 9, except that correlations are derived, based on the sample with the 300 coldest (a,b) and 300 warmest (c,d) complete seasons over the eastern Mediterranean in the CTRL run. Correlations are shown for a)-b) meridional wind, c)-d) precipitation.

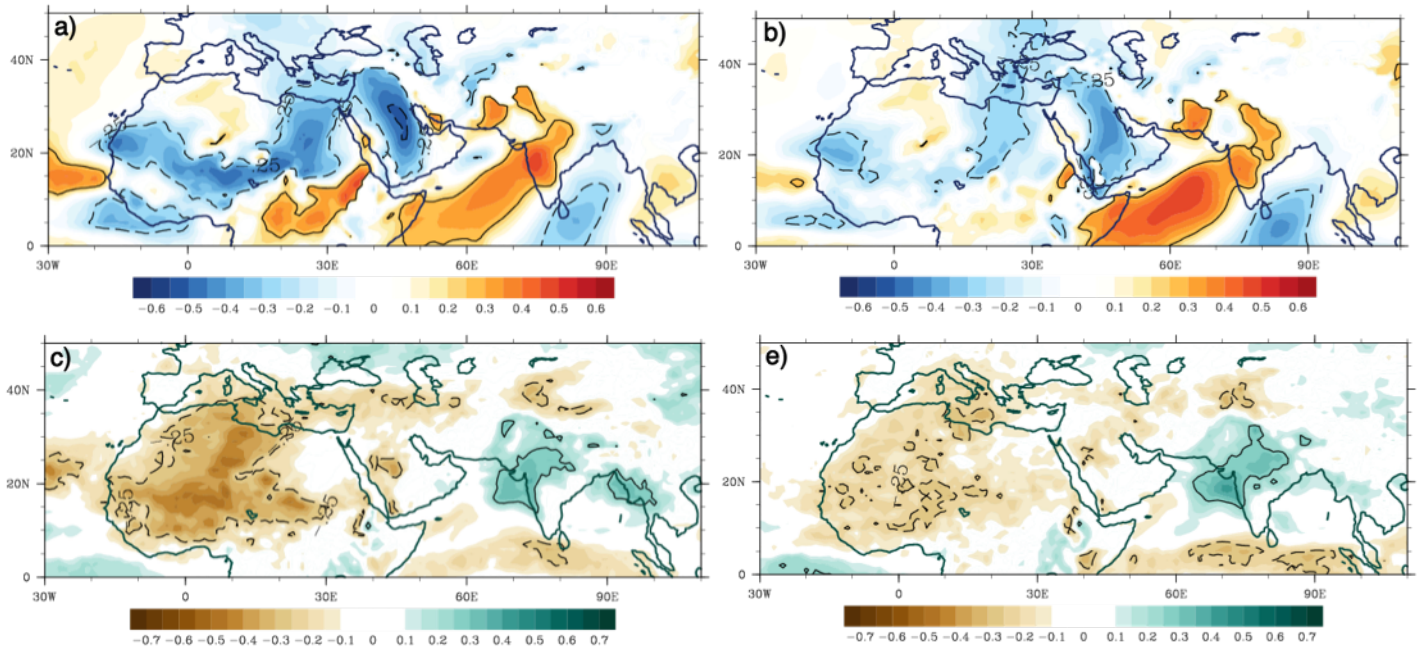

Fig S7. As in Fig 10c, except that for a) June, b) August, and for a larger domain.

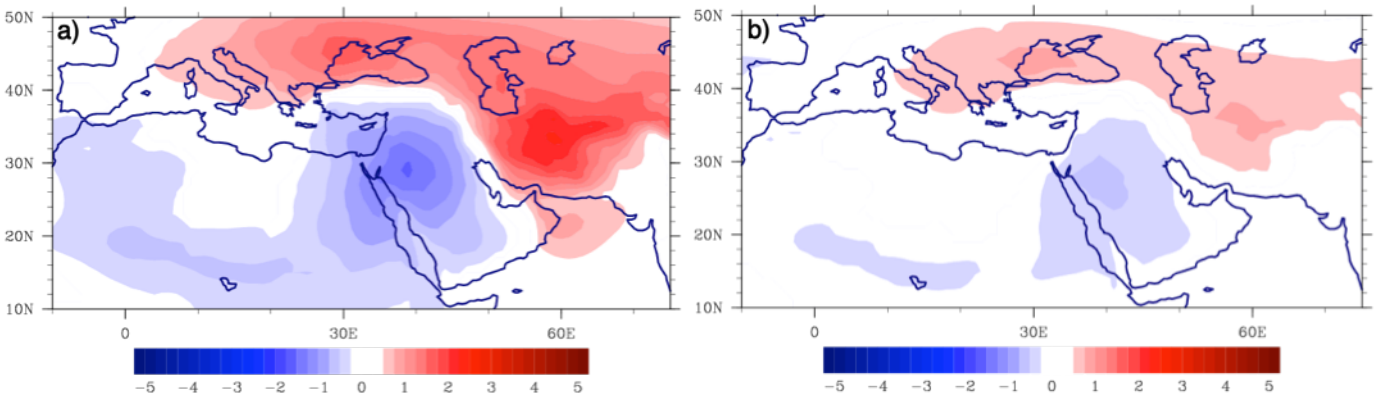

Fig S8. As in Fig 10c, except that the regions used for differentiation between warmest and coolest seasons are larger: a) 0°-40°E, 30°-36°N, b) 20°-40°E, 30°-36°N, c) 30°-50°E, 30°-36°N, d) 30°-50°E, 30°-40°N, e) 30°-50°E, 30°-45°N.

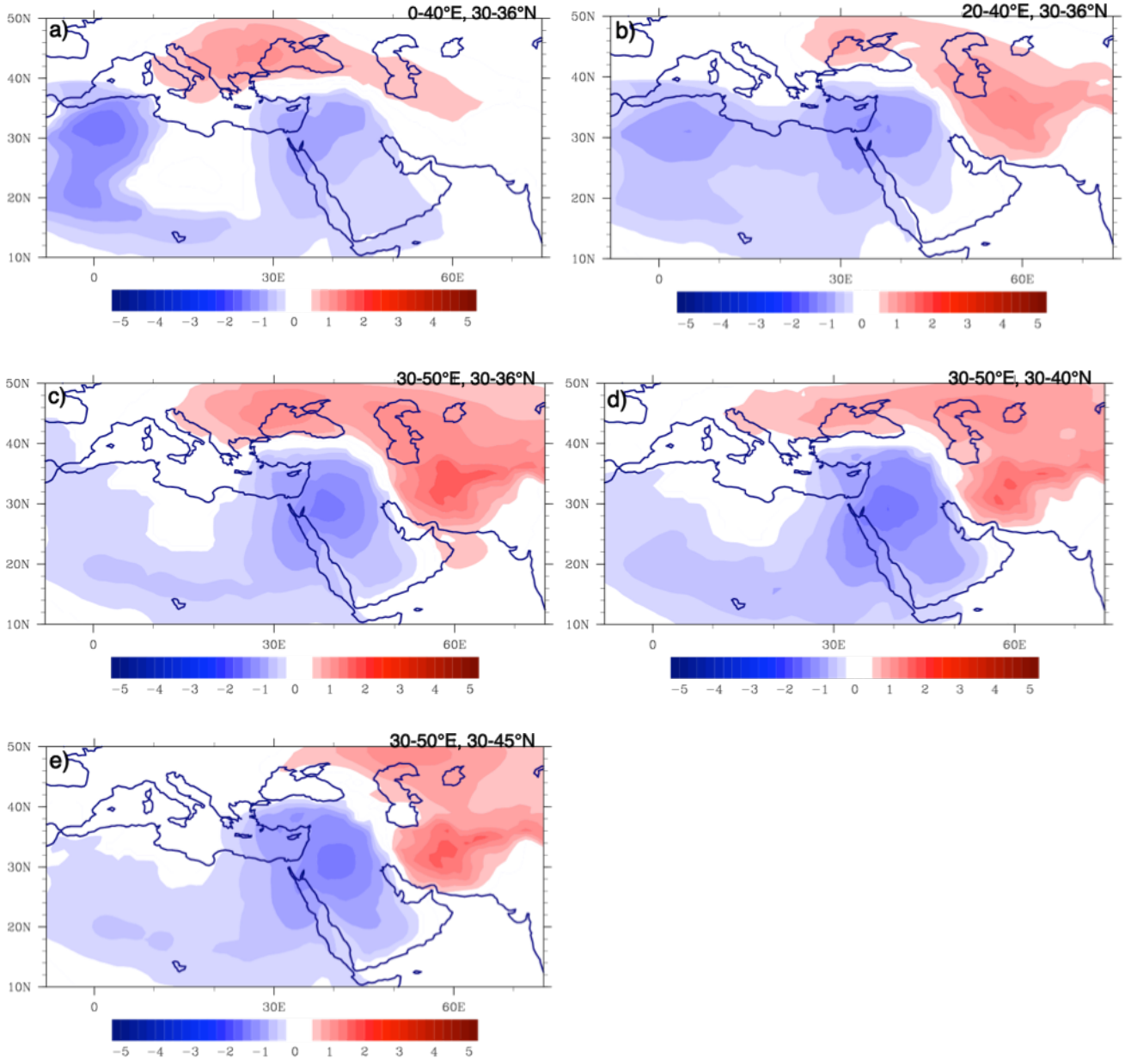

Fig S9. Correlations between the principal component time series of EOF1 omega over EMED and precipitation in (a) June, (b) July (as in Figure 6f), (c) August. Solid lines denote positive correlations, and stippled denote negative correlations, both for the absolute values larger, than 0.25.